

THE FORMATION OF SHELL GALAXIES SIMILAR TO NGC 7600 IN THE COLD DARK MATTER COSMOGONY

ANDREW P. COOPER

Max Planck Institut für Astrophysik, Karl-Schwarzschild-Str. 1 85741 Garching, Germany

DAVID MARTÍNEZ-DELGADO

Max Planck Institut für Astronomie, Königstuhl 17 D-69117, Heidelberg, Germany

JOHN HELLY, CARLOS FRENK, SHAUN COLE

Institute For Computational Cosmology, Department of Physics, University of Durham, South Road, DH1 3LE, Durham, UK

KEN CRAWFORD

Rancho del Sol Observatory, Camino, CA 95709, USA

STEFANO ZIBETTI

Dark Cosmology Centre, Niels Bohr Institute - University of Copenhagen Juliane Maries Vej 30, DK-2100 Copenhagen, Denmark

JULIO A. CARBALLO-BELLO

Instituto de Astrofísica de Canarias, La Laguna, Spain

AND

R. JAY GABANY

Black Bird Observatory II, California, USA

Draft version October 30, 2018

ABSTRACT

We present new deep observations of ‘shell’ structures in the halo of the nearby elliptical galaxy NGC 7600, alongside a movie of galaxy formation in a cold dark matter universe (<http://www.virgo.dur.ac.uk/shell-galaxies>). The movie, based on an ab initio cosmological simulation, shows how continuous accretion of clumps of dark matter and stars creates a swath of diffuse circumgalactic structures. The disruption of a massive clump on a near-radial orbit creates a complex system of transient concentric shells which bare a striking resemblance to those of NGC 7600. With the aid of the simulation we interpret NGC 7600 in the context of the CDM model.

Subject headings: galaxies: elliptical and lenticular, cD — galaxies: halos — galaxies: individual (NGC 7600) — galaxies: kinematics and dynamics — galaxies: peculiar — galaxies: structure

1. INTRODUCTION

Deep observations of nearby galaxies have uncovered a wealth of faint circumgalactic streams, shells and other structures (e.g. McConnachie et al. 2009; Martínez-Delgado et al. 2010). Such features are a natural occurrence in the cold dark matter (CDM) cosmogony, in which the dark haloes hosting massive galaxies continually accrete and disrupt their smaller companions. Cooper et al. (2010, hereafter C10) have carried out ultra-high resolution simulations of this process using six N-body models of Milky Way-mass dark matter haloes from the Aquarius project (Springel et al. 2008). Using the GALFORM semi-analytic model of galaxy formation to calculate the epoch and location of star formation in the simulation, C10 tagged dark matter particles in appropriate regions of phase-space to follow the dynamical evolution of stars stripped from the progenitors

of these haloes. In this way, they were able to model the build-up of galactic stellar haloes through the tidal disruption of satellite galaxies.

In this paper, we present a movie¹ from one of the six simulations of C10 (Aq-F-2). The movie is a compelling illustration of the complexity and dynamism of structure formation in CDM. Because of this complexity, full cosmological modeling is essential – a conclusion emphasized by our movie.

The stellar halo of Aq-F-2 contains an extensive system of interleaved ‘shells’. Examples of stellar haloes with this distinctive morphology have been known for decades (e.g. Arp 1966; Malin & Carter 1983) and their fainter analogs seem to be common in the local universe (e.g. Martínez-Delgado et al. 2010; Tal et al. 2009). In this paper we present a new deep panoramic image of the diffuse light around one such galaxy, NGC 7600, showing

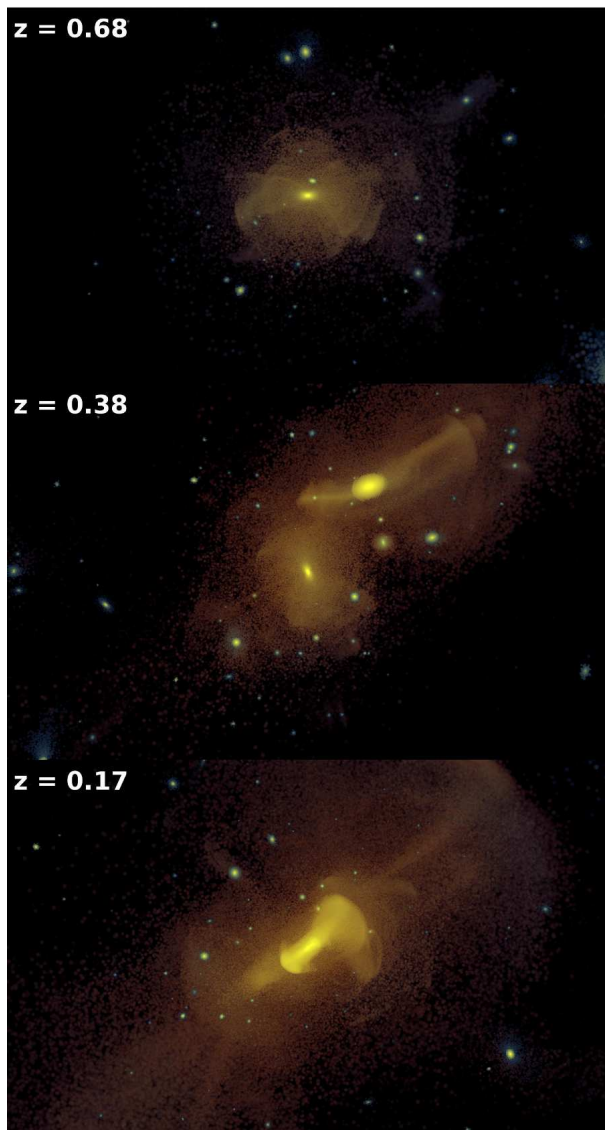


Figure 1. The evolution of the stellar halo in the Aq-F-2 simulation (Cooper et al. 2010). These are still frames from the movie available in the electronic edition of the Journal, and show stages in the formation of the shell system at redshifts $z = 0.68, 0.38$ and 0.17 , corresponding to lookback times of 6, 4 and 2 Gyr respectively. The final state is shown in Fig. 2. Brightness corresponds to projected stellar mass surface density. Colors, ranging from dark blue to yellow, correspond to velocity dispersion (from ~ 50 – 315 km s^{-1}). All images are centered on the main halo and the field of view in each image is approximately 256 kpc by 160 kpc (comoving). Only accreted stars are shown; the majority of the stars in the central galaxy do not appear in these images – see text and the caption of Fig. 2 for further details.

its well-known shell system and previously undetected faint features. Even though our ab initio simulation was not constrained to reproduce NGC 7600 in any way, the observations and the simulation are strikingly similar, suggesting that such systems arise naturally in the CDM model.

The movie shows how the simulated system is formed in a major (3 : 1) merger between a $\sim 10^{12} M_{\odot}$ halo and its brightest satellite at $z \sim 0.4$. At $z = 0$, our semi-analytic model predicts that this halo hosts an ellipsoidal galaxy (bulge-to-total mass ratio $B/T = 0.85$) of total stellar mass $1.3 \times 10^{10} M_{\odot}$.

2. THE MOVIE

Three still frames from our movie are shown in Fig 1. The GALFORM model follows the formation of the entire galaxy (disk, bulge, halo; see C10 for details), but the movie shows only the evolution of the stars formed in (and stripped out of) all progenitors of the final galaxy *except for* the main progenitor. Stars formed *in situ* – those that would make up all of the disk and part of the bulge – are *not* included in our particle-tagging procedure and are *not* shown.

The movie begins with the close encounter of two dark matter haloes at $z = 4$. These haloes merge after ~ 2.5 Gyr ($z = 2.7$). Both are surrounded by a number of dwarf galaxies and the debris of earlier mergers. The halo entering the picture from below is the more massive. As the haloes coalesce, their cores oscillate radially about the center of the potential, creating a series of compact shells (density caustics at the apocenters of approximately radial stellar orbits; Quinn 1984). This merger establishes the main halo, on which the movie is centered for the remainder of the simulation. The shells propagate rapidly outwards and by $z = 2$ have phase-mixed into a diffuse bow-tie-shaped cloud.

In the next phase of the movie ($z = 2 - 0.5$, spanning ~ 5 Gyr – see the topmost panel of Fig. 1) the halo is bombarded by a number of smaller satellites on high-angular-momentum orbits. Tidal forces disrupt many of these satellites, leaving behind streams of debris that crisscross the halo. As with the shells seen earlier, the stars in these streams pile up at the apocenters of their orbits. Where the stream progenitor crosses the center of the halo perpendicular to the line of sight, it appears as an ‘umbrella’: a broad arc at the end of a thin stream (e.g. Martínez-Delgado et al. 2010). These features are rapidly erased by phase-mixing, perturbations to the potential and the decay of satellite orbits through dynamical friction.

The final and most spectacular stage of the movie begins at $z = 0.4$. As shown in the central panel of Fig. 1, a bright satellite appears in the upper right of the frame.

The satellite (whose stellar mass of $\sim 7 \times 10^6 M_{\odot}$ at $z = 0.4$ is only $\sim 0.1\%$ of the stellar mass of the main galaxy at that time, although its dark matter halo is $1/3$ of the main dark matter halo) seems much brighter than the central galaxy because only stars *accreted* by the central galaxy are shown – GALFORM predicts that the majority of its stars form in situ, and these are not tagged by dark matter particles in our model (see C10). The satellite galaxy brings with it its own extensive stellar halo and set of companions, one of which is already being disrupted into a wide stream when its host arrives in the main halo. The bright satellite makes two pericentric passages as the angular momentum is drained from its orbit. These early passages strip the satellite of its stellar halo and its companions. Meanwhile, the stellar halo of the main galaxy is distorted and mixed by the new arrival, destroying pre-existing tidal features.

What happens next ($z \sim 0.27$, lowest panel of Fig 1.) is crucial for understanding NGC 7600. The bright satellite is now on an approximately radial orbit and will pass through the center of the potential at subsequent pericenters. Material is stripped from the satellite on each of these passages, just like the stellar streams. Here, how-

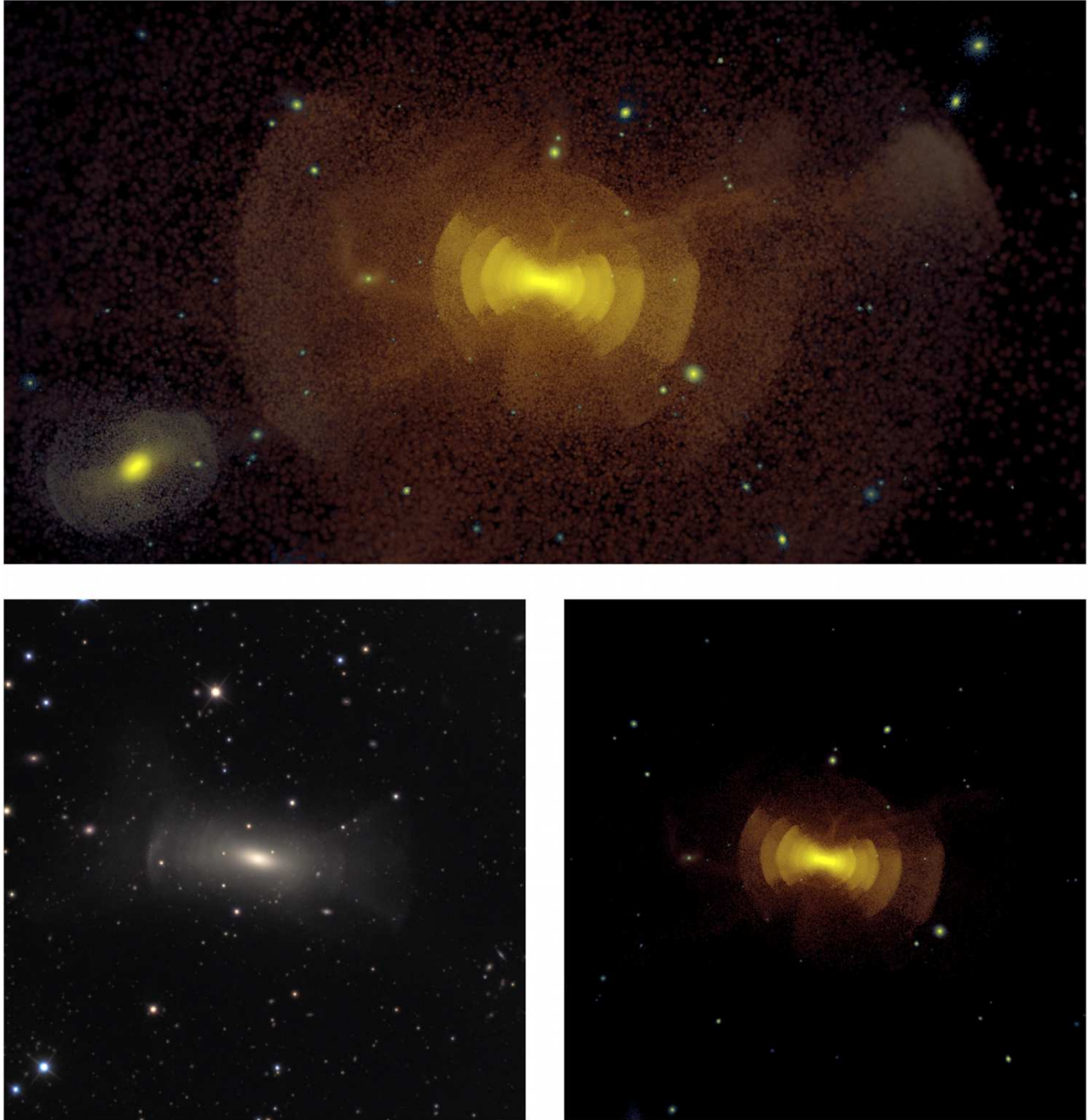


Figure 2. *Top:* final ($z = 0$) frame of the movie. The brightness scale (surface mass density) was chosen to show the full extent of the structure in the simulation. Color (from blue to yellow) corresponds to velocity dispersion. Only *accreted* stars are shown so the central concentration of light corresponds to the small fraction of bulge stars that were stripped from satellites. *Bottom left:* a deep image of NGC 7600 obtained with the Rancho del Sol 0.5-meter telescope. North is up, East is left. The original image (see Fig. 3) has been cropped. The total field of view is $12' \times 12'$ ($\sim 175 \times 175$ kpc). *Bottom right:* the same field of view in Aq-F-2, with a brightness scale chosen to match the extent of the visible structure around NGC 7600.

ever, liberated stars fan out over a cone of radial orbits. This is the same phenomenon that created the shells at $z = 2.3$, although here the orbital energy of the satellite is much greater and the outer shells are much more extensive. As described by Quinn (1984), stars liberated on a given passage have a range of binding energies with respect to their host (determined by the structure of the progenitor and the interaction of the two potentials). Stars with low binding energies have longer orbital periods and turn around at larger radii than more tightly-bound stars. Thus, the outermost shell forms

first, from the loosely-bound stars that lead the satellite along its orbit. All shells move outward with time as stars with ever-longer periods reach apocentre. At any given instant, the edges of the shells are composed of stars that have executed an integer number of orbits (see e.g. Merrifield & Kuijken 1998). They are interleaved in radius on either side of the center.

Finally, note that the companion that was already disrupting around the shell progenitor when it entered the main halo embarks on an independent orbit after the first pericentric passage. This satellite is continually stripped

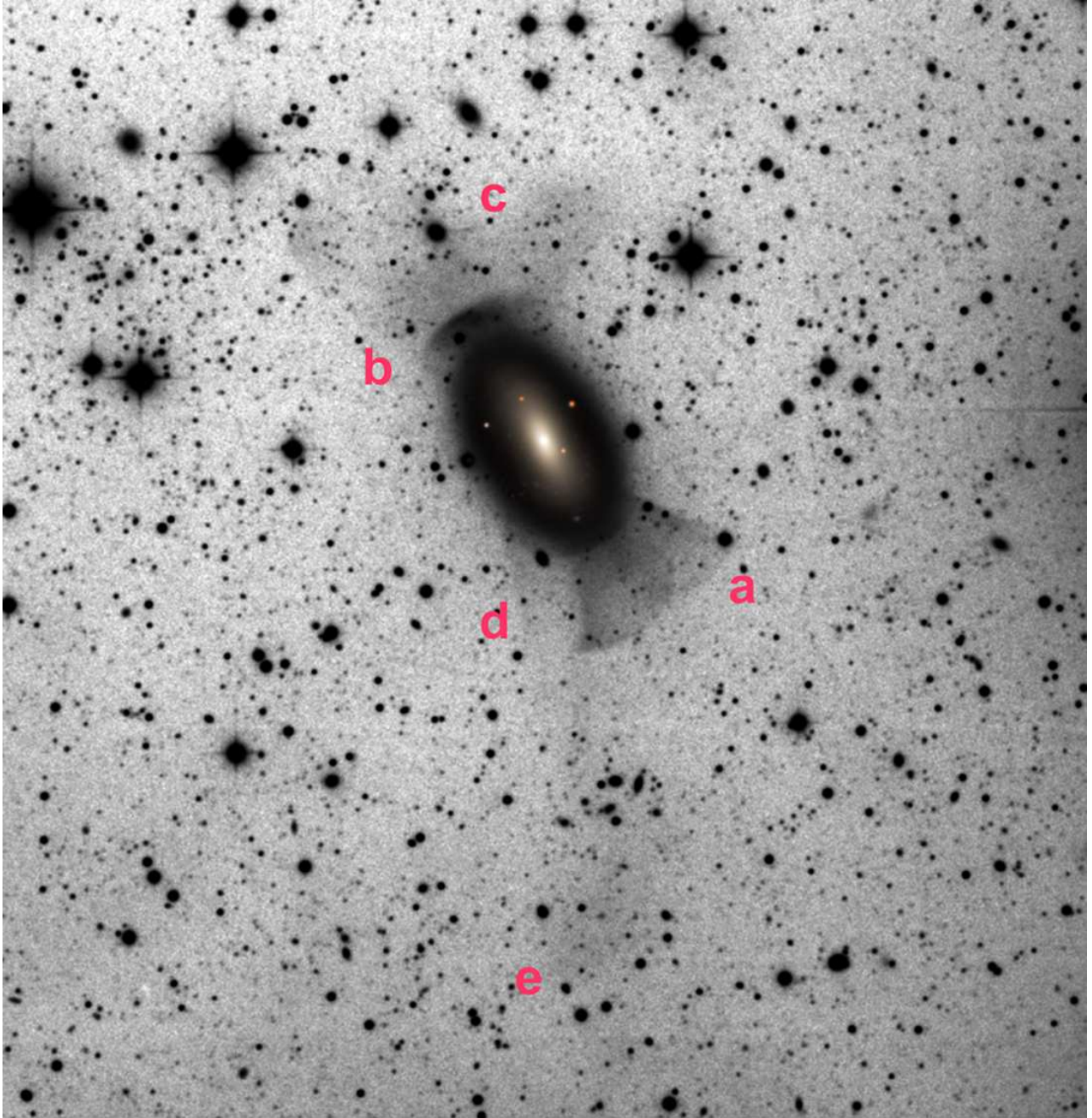


Figure 3. A super-stretched, wide field view of the stellar debris around NGC 7600. The field of view is $18.5' \times 18.9'$ ($268 \text{ kpc} \times 274 \text{ kpc}$). The major axis of the galaxy and its shells lies along the East-West direction (top left to bottom right). A color image of the central region of the galaxy is superimposed on the saturated portion of the image. Labels *a* and *b* mark the shells visible in Fig. 2. Other fragments of debris described in the text are labeled *c-e*. The label *e* is 140 kpc in projection from the center of the galaxy.

of its stars, which form a number of umbrellas with very similar radius and curvature to the shells. At the last apocentre before its complete disruption ($z \sim 0.09$), the debris stream of this satellite lies perpendicular to the shell axis. The movie rotates around the halo to show the flattened conical geometry of the shell system and its dramatically different appearance from different viewing angles.

3. THE NEARBY GALAXY NGC 7600

NGC 7600 ($D = 50 \text{ Mpc}$; $M_B = -20.27 \pm 0.52$) is a nearby elliptical galaxy (classified visually as S0, but

without a disk; Dressler & Sandage 1983). Its stellar mass, obtained from the method of Zibetti et al. (2009), is $(6.35 \pm 1.19) \times 10^{10} M_\odot$, similar to the stellar mass of the Milky Way. Deep photographic plates processed by Malin & Carter (1980) revealed an interleaved system of sharp-edged shells, which are roughly aligned with the major axis of the galaxy (Schweizer & Seitzer 1988). These shells can be seen in the lower left panel of Fig. 2, where we present a new deep image of NGC 7600 obtained using the techniques described in Martínez-Delgado et al. (2010). Our new image also re-

veals a number of fainter features not previously seen. Appendix A contains full details of these observations.

The complex field of tidal debris in the outer halo of NGC 7600 is better seen in the super-stretched, wide field image in Fig. 3. In this image the inner shell structure visible in Fig. 2 is saturated, and only two external shells can be discerned, one on either side of the galaxy. The bright shell West of the galaxy, labeled *a* in Fig. 3, corresponds to the outermost feature visible in Fig. 2. Our deep image reveals two further giant cones of material West of the galaxy, which are not as clearly aligned with the major axis. Fragments of these structures were also reported by Turnbull et al. (1999).

Fig. 3 reveals several features that have not been reported so far. A diffuse system of debris clouds is visible to the Northeast (labeled *c* in Fig. 3). It seems to consist of three components, extending up to 110 kpc from the center of the galaxy. A narrow ‘spike’ emerges from the diffuse halo (labeled *d*). Finally, we detect a large diffuse stellar cloud (labeled *e*) $\sim 9.7'$ from the galaxy, corresponding to a projected distance of 140 kpc. An extremely faint narrow feature seems to connect this cloud to the main body of NGC 7600. Together, this diversity of tidal features suggests that NGC 7600 has undergone an active and complex merging history in the recent past.

There is an extremely close correspondence between NGC 7600 and the diffuse structures seen in the Aq-F-2 simulation. Not only are the morphological similarities striking, but the inner shells in the simulation have comparable surface brightness to those of NGC 7600, $\sim 27 \text{ mag arcsecond}^{-2}$, according to the population synthesis model used by C10. This is particularly remarkable since the model galaxy was in no way constrained to resemble NGC 7600.

4. DISCUSSION

The evolution of Aq-F-2 depicted in the movie highlights several interesting aspects of the formation of systems analogous to NGC 7600 in a CDM cosmogony.

The first remarkable feature is the complexity of the shell system itself. The merger origin of circumgalactic shells was first described in detail by Quinn (1984), who concluded that the shell progenitor must be a cold stellar system on a radial orbit, as is approximately the case for the shell progenitor in Aq-F-2. (Few orbits are perfectly radial to begin with, and, in fact, our shell progenitor passes pericenter twice before its orbit is aligned and shells are produced.)

The earliest models of shell galaxies were based on simplifying assumptions and restricted N-body simulations (e.g. Dupraz & Combes 1986). In the simplest case, a single instantaneous disruption event liberates all the stars from the progenitor. The outermost shell is formed first, and successive shells are created by phase-wrapping. In our simulation, however, the core of the shell progenitor survives through several pericenters. In the first few passages, the ‘new’ shells appearing are, in fact, the *first* shells of *separate* shell systems – one per pericentric passage of the core. Only later do phase-wraps of these multiple shells systems begin to appear.

Indeed, the system is even more complex. In the self-consistent potential of our simulation, energy is exchanged between the shell progenitor, the main halo and the liberated stars. Heisler & White (1990) pointed out

that interactions between the shell progenitor and its tidal stream (the ‘stalk’ intermittently visible along the shell axis) leads to the decay of the satellite’s orbit independently of dynamical friction against the host (both processes take place here). From our simulation it is clear that the orbit of the satellite decays significantly before its final disruption.

The evolution in the orbit of the shell progenitor gradually changes the alignment of new shells throughout the merger. NGC 7600 is highly elliptical and well-aligned with its innermost shells (Turnbull et al. 1999). The outer shells visible in Fig. 3 show tentative evidence for misalignment. In the simulation, the innermost shells (the last to be created) are also aligned with the major axis of the central bulge. The accreted stars in the final system have large velocity dispersions ($\sigma > 100 \text{ km s}^{-1}$), and exhibit only weak bulk rotation about the halo center ($v_{\text{rot}} \sim 10 \text{ km s}^{-1}$).

Over the course of the simulation, the morphology of the stellar halo goes through several short-lived transformations. Many prominent features are easily disrupted when the central potential is strongly perturbed. Even the dominant shell system in Aq-F-2 is evolving rapidly. The first shells created in the merger have already phase-mixed away by $z = 0$.

Finally, the shell progenitor in Aq-F-2 is a relatively massive dwarf satellite which enters the main halo along with a number of even smaller galaxies. This ‘correlated infall’ is characteristic of the CDM model (e.g. Libeskind et al. 2005; Li & Helmi 2008). Not only are individual bright satellites likely to have several luminous companions, but *most* of these groups, large and small, are accreted along filaments of the cosmic web. This correlates the directions from which infalling satellites are accreted with the shape of the dark matter halo (Lovell et al. 2011; Vera-Ciro et al. 2011). Some of the satellites of the shell progenitor are already suffering tidal disruption before the system is accreted into the main halo. The brightest of these creates a perpendicular umbrella feature resembling a shell.

5. CONCLUSION

We have presented a new deep image of NGC 7600 revealing new tidal features in its outer regions. The distribution of stellar debris in this image is strikingly similar to that of the Aq-F-2 simulation shown in the movie that accompanies this paper. The simulation suggests a likely scenario for the formation of the observed shell system in NGC 7600 and gives a deeper insight into the violent nature of galaxy assembly in CDM.

Our simulation confirms the established hypothesis that shells are created by the disruption of a satellite system on a radial orbit (here the satellite is spheroidal, but disk-like progenitors are also possible). However, in our simulation, the evolution of the orbit of the main shell progenitor is complex, tidal structures are transient and interact with one another, and shell-like features are contributed by more than one progenitor. (Even many of the satellite galaxies around Aq-F-2 themselves show miniature shell systems.) That we find one such example among six randomly selected $\sim 10^{12} M_{\odot}$ haloes suggests that such mergers and complex shells are a natural expectation of the CDM model. Deeper observations of nearby galaxies should reveal many more cases.

Although the prevalence of shell systems and their dependence on galaxy properties remains to be quantified, both in the real universe and in simulations, it is clear that these features offer the prospect of a novel test of the CDM model on galactic scales. These scales are the most sensitive to fundamental properties of the dark matter, for example to whether the dark matter is cold or warm. Hierarchical formation – the hallmark of cold dark matter – must be accompanied by the formation of shells, a process that is testable with deep, wide-field observations of nearby galaxies.

DMD thanks the Max-Planck Institute for Astrophysics for hospitality during the preparation of this work. CSF acknowledges a Royal Society Wolfson Research Merit Award and ERC Advanced Investigator grant 267291 COSMIWAY. SMC acknowledges a Leverhulme Fellowship. The Dark Cosmology Centre is funded by the Danish National Research Foundation. Calculations for this paper were performed on the ICC Cosmology Machine, part of the DiRAC Facility, the Leibniz Rechenzentrum (Garching) and LOFAR/STELLA (Groningen). This work was supported in part by an STFC rolling grant to the ICC.

APPENDIX

OBSERVATIONS AND DATA REDUCTION

We have obtained new deep optical images of NGC 7600 with the 0.508 m Ritchey-Chrétien telescope of the Rancho del Sol Observatory in Camino, California. We used an Apogee Alta u9000 CCD camera (pixel size 12 micron), providing a field of view of $29.3' \times 29.3'$ at a plate scale of $0.58'' \text{ pixel}^{-1}$. Our image set consists of 34 individual exposures of 20 minutes each with a clear luminance filter ($3500 < \lambda < 8500$). These dark-sky images were obtained between September 2nd and September 9th, 2010. They were reduced using standard procedures for bias correction and flatfield, as explained in Martínez-Delgado et al. (2009). The final image was obtained by summing all the luminance CCD exposures, with a total accumulated exposure time of 680 minutes (11.33 hours).

We performed a careful subtraction of the background in the final reduced image. On large scales, the background is heavily affected by the scattered light of bright sources and other artifacts (possibly due to internal reflections in the camera). For this reason, we optimize the subtraction within $\sim 8'$ from the galaxy center. We select 36 boxes around the galaxy, chosen not to include bright stars or be contaminated by the galaxy halo and the faint diffuse features. A first degree 2-dimensional polynomial is fit to the pixels in these regions using a very conservative sigma-clipping, and subtracted from the image to remove background gradients. We further subtract the residual pedestal given by the median counts of pixels in the selected regions.

An obvious disadvantage of luminance images is the lack of a photometric standard system for direct calibration of the flux. For this purpose we use images of the same sky area from the Sloan Digital Sky Survey (SDSS DR8, Aihara et al. 2011) to calibrate our luminance image in the SDSS photometric system (specifically the g , r and i bands that cover the spectral range

of the luminance filter). To reduce the uncertainty due to the unknown color terms, we calibrate our image on the brightest regions of NGC 7600 (within $\sim 1'$) and assume that the faint features have similar colors to the main galaxy body (as suggested by Turnbull et al. 1999). From the noise properties of the background we derive a 3σ threshold for feature detections over $2''$ apertures of 28.1, 27.3 and 26.9 mag arcsec $^{-2}$ in g , r and i bands, respectively. The 1σ accuracy of the background subtraction is estimated from the box-to-box variance of the average residual surface brightness in 29.7, 28.9 and 28.5 mag arcsec $^{-2}$ in g , r and i bands, respectively.

We derive a mass-to-light ratio from the H -band luminosity and $(g - i, i - H)$ colors of NGC 7600, using the lookup tables of Zibetti et al. (2009), and estimate a stellar mass of $6.35 \times 10^{10} \pm 1.91 M_{\odot}$. H is taken from 2MASS, g and i from SDSS. All photometry is integrated within the elliptical isophote corresponding to 25mag arcsec $^{-2}$ in the SDSS r band (150 min semi-major axis, $b/a = 0.39$). We assume a distance modulus of 33.18. Photometric quantities (corrected for foreground galactic extinction) are: $m_g = 12.12$, $m_r = 11.44$, $m_i = 11.03$, $m_H = 8.79$ (Vega). The H-band luminosity is $1.27 \times 10^{11} L_{\odot}$.

REFERENCES

- Aihara, H., et al. 2011, ApJS, 193, 29
 Arp, H. 1966, ApJS, 14, 1
 Bower, R. G., et al. 2006, MNRAS, 370, 645
 Bullock, J. S., & Johnston, K. V. 2005, ApJ, 635, 931
 Cooper, A. P., et al. 2010, MNRAS, 406, 744
 Dupraz, C., & Combes, F. 1986, A&A, 166, 53
 Dressler, A., & Sandage, A. 1983, ApJ, 265, 664
 Heisler, J., & White, S. D. M. 1990, MNRAS, 243, 199
 Hernquist, L., & Quinn, P. J. 1989, ApJ, 342, 1
 Johnston, K. V., Bullock, J. S., Sharma, S., Font, A., Robertson, B. E., & Leitner, S. N. 2008, ApJ, 689, 936
 Li, Y.-S., & Helmi, A. 2008, MNRAS, 385, 1365
 Libeskind, N. I., Frenk, C. S., Cole, S., Helly, J. C., Jenkins, A., Navarro, J. F., Power, C., 2005, MNRAS, 363, 146
 Lovell, M. R., Eke, V. R., Frenk, C. S., & Jenkins, A. 2011, MNRAS, 413, 3013
 Malin, D. F., & Carter, D. 1980, Nature, 285, 643
 Malin, D. F., & Carter, D. 1983, ApJ, 274, 534
 Martínez-Delgado, D., Pohlen, M., Gabany, R. J., Majewski, S. R., Peñarrubia, J., & Palma, C. 2009, ApJ, 692, 955
 Martínez-Delgado, D., et al. 2010, AJ, 140, 962
 McConnachie, A. W., et al. 2009, Nature, 461, 66
 Merrifield, M. R., & Kuijken, K. 1998, MNRAS, 297, 1292
 Nulsen, P. E. J. 1989, ApJ, 346, 690
 Quinn, P. J. 1984, ApJ, 279, 596
 Schweizer, F., & Seitzer, P. 1988, ApJ, 328, 88
 Schweizer, F., & Seitzer, P. 1992, AJ, 104, 1039
 Sikkema, G., Carter, D., Peletier, R. F., Balcells, M., Del Burgo, C., & Valentijn, E. A. 2007, A&A, 467, 1011
 Springel, V., et al. 2005, Nature, 435, 629
 Springel, V., et al. 2008, MNRAS, 391, 1685
 Tal, T., van Dokkum, P. G., Nelan, J., & Bezanson, R. 2009, AJ, 138, 1417
 Turnbull, A. J., Bridges, T. J., & Carter, D. 1999, MNRAS, 307, 967
 Vera-Ciro, C. A., Sales, L. V., Helmi, A., et al. 2011, MNRAS, 416, 1377
 Zibetti, S., Charlot, S., & Rix, H.-W. 2009, MNRAS, 400, 1181